CHAPTER-3

NUMERICAL AND EXPERIMENTAL METHODOLOGY

3.1 NUMERICAL MODELLING OF CAVITATION

To simulate cavitating flow, two types of models are commonly used: two-fluid models, which treat liquid and vapour separately, and continuous flow approaches, which employ a homogenous combination of both. An equation of state is used in continuum flow methods to describe phase change and cavitation growth. This study uses a homogeneous equilibrium model (HEM) to simulate fuel flow inside injectors. In the present study; the governing equations are solved using commercial computational fluid dynamics code ANSYS-Fluent. The essential idea behind homogeneous models is that relative motion between phases can be ignored. In the event of a sufficiently well-mixed two-phase flow, the dispersed particle size is small enough to eliminate considerable relative motion. Without relative motion, the mass and momentum conservation equations for inviscid, homogeneous flow simplify to a single-phase form:

$$\frac{\partial \rho}{\partial t} + \frac{\partial (u_j \rho)}{\partial x_j} = 0 \tag{3.1}$$

$$\frac{\partial (\rho u_i)}{\partial t} + \frac{\partial (\rho u_i u_j)}{\partial x_j} = -\frac{\partial p}{\partial x_i} + \frac{\partial}{\partial x_j}\left[\mu_{eff}\left(\frac{\partial u_i}{\partial x_j} + \frac{\partial u_j}{\partial x_i} - \frac{2}{3}\frac{\partial u_i}{\partial x_i}\right)\right] \tag{3.2}$$

Where ρ is the mixture density. The volume fraction of the liquid phase is used to calculate the mixture density and mixture viscosity.

$$\rho = (1 - \alpha_l)\rho_v + \alpha_l \rho_l \tag{3.3}$$

$$\mu = (1 - \alpha_l)\mu_v + \alpha_l \mu_l \tag{3.4}$$

Where ρ_v and ρ_l are the vapor phase and liquid phase density, and μ_v and μ_l are the vapor phase and liquid phase viscosity, respectively. The effective viscosity (μ_{eff}) is the summation of the molecular viscosity (μ_m) and turbulent viscosity (μ_t). The turbulent viscosity can be calculated by:

k-ε models

$$\mu_t = C_\mu \rho \frac{k^2}{\varepsilon} \tag{3.5}$$

k − ω models

$$\mu_t = \alpha \rho \frac{k}{\omega} \tag{3.6}$$

A source term is required in the continuity equation to evaluate the phase change between liquid and vapor with this model.

$$\frac{\partial(\alpha_l \rho_l)}{\partial t} + \nabla \cdot (\alpha_l \rho_l U) = R_c + R_e \tag{3.7}$$

Where R_c and R_e are the source term to calculate the rate of mass transfer for condensation and evaporation, respectively. U, α_l, and ρ_l are mixture velocity, the volume fraction of liquid and density of liquid respectively. If there is no mass transfer between phases, RHS is zero, the transport equation for the Volume of Fluid (VOF) model. The volume fraction of the vapor phase (α_v) is calculated by:

$$\alpha_v = 1 - \alpha_l = \frac{\frac{4}{3}\pi R_b^3 n_0}{1 + \frac{4}{3}\pi R_b^3 n_0} \tag{3.8}$$

Where $R_b$and n_0 denote the bubble radius and bubble nuclei number density (bubble concentration per unit volume). The growth & collapse of the bubbles can be calculated by using the Rayleigh-Plesset (RP) bubble dynamic equation.

$$R\frac{d^2R}{dt^2} + \frac{3}{2}\left(\frac{dR}{dt}\right)^2 + \frac{4\mu}{R}\frac{dR}{dt} + \frac{2\sigma}{\rho R} = \frac{P_v - P_\infty}{\rho} \tag{3.9}$$

Where R is the bubble radius, $\frac{dR}{dt}$is the bubble wall velocity, σ is the surface tension, and P_v is the vapor pressure. The RP equation considers vapor pressure (P_v) as a threshold for evaporation and condensation. The mass transfer rate is given in the Table 3.1.

Table 3.1 Different mass transfer source terms for condensation and evaporation

Evaporation ($P_L < P_V$)		
Schnerr-Sauer [40]	$R_e = -C_v \frac{3\rho_l\rho_v}{\rho_m}\frac{\alpha_l(1-\alpha_l)}{R_b} sgn(P_l - P_v)\sqrt{\frac{2\lvert P_l - P_v\rvert}{3\rho_l}}$	(3.10)
Zwart et al. [42]	$R_e = F_{vap}\frac{3\alpha_{nuc}\rho_v(1-\alpha_v)}{R_b}\sqrt{\frac{2\lvert P_l-P_v\rvert}{3\rho_l}}$ (F_{vap}=50)	(3.11)
Condensation ($P_V < P_L$)		
Schnerr-Sauer [40]	$R_c = C_c \frac{3\rho_l\rho_v}{\rho_m}\frac{\alpha_l(1-\alpha_l)}{R_b} sgn(P_v - P_l)\sqrt{\frac{2\lvert P_l - P_v\rvert}{3\rho_l}}$	(3.12)
Zwart et al. [42]	$R_c = F_{con}\frac{3n_0\rho_v}{R_b}\sqrt{\frac{2\lvert P_l-P_v\rvert}{3\rho_l}}$, ($F_{con}$=0.01)	(3.13)

The interface between the liquid and vapour can be capture by using the sharp interface modelling. It required solving a single momentum equation in which fluid properties are the function of volume of fraction. In the right-hand side, the source term ($f_\sigma\delta_S$) to consider the surface tension force at the interface between two phases.

$$\frac{\partial(\rho u_i)}{\partial t}+\frac{\partial(\rho u_i u_j)}{\partial x_j}=-\frac{\partial p}{\partial x_i}+\frac{\partial}{\partial x_j}\left[\mu_{eff}\left(\frac{\partial u_i}{\partial x_j}+\frac{\partial u_j}{\partial x_i}-\frac{2}{3}\frac{\partial u_i}{\partial x_i}\right)\right]+\mathrm{f}_\sigma\delta_\mathrm{s} \quad (3.14)$$

3.2 NUMERICAL MODELLING OF SPRAY

In the present work, ANSYS-FLUENT was employed to study non-evaporating spray. FLUENT provides a discrete phase model (DPM) to simulate spray characteristics, which is based on the Lagrangian drop Eulerian fluid method. It allows for tracking the fuel droplets (discrete phase) in the Lagrangian frame of reference and the continuous gas phase in the Eulerian frame of reference. Furthermore, the Wave breakup model, proposed by Reitz et al. [7] has been used to capture droplet breakup phenomena. The Wave model is suitable for high Weber numbers (We>100) and high-pressure spray. When the fuel droplets travel in the chamber, they experience the turbulent vortex, which causes the motion of the particles to shift from straight lines to non-smooth curves. The interaction between the droplet and discrete vortex is taken into account by the discrete random walk (DRW) model. The discrete random walk model was used to simulate the turbulent diffusion of the spray droplets.

3.2.1 Discrete phase model (DPM)

The transport equations are solved for continuous flow in the Euler frame of reference, while discrete phase particles are used to simulate spray formation in a Lagrangian frame of reference. The spherical particle introduced in to the continuous phase & trajectory is calculated by two-way coupling. The trajectories of the discrete particles are calculated by the force balance on particles given by:

$$\frac{\partial u_p}{\partial t}=F_D(u_a-u_p)+g_x\frac{\partial(\rho_p-\rho_a)}{\rho_p}+F_x \quad (3.15)$$

Where ρ_p&ρ_a are the density of particles and air respectively, u_p&u_a are the velocity of particles and air, F_x is the additional force interact on particle due to mass, acceleration and pressure & F_D is the drag force acting on the particle given by:

$$F_D=\frac{1}{2}\rho A_p C_D(u_a-u_p) \quad (3.16)$$

Where,$A_p$cross sectional area of particle in mm, $C_D$is the drag coefficient of the particle calculated from the Schiller and Naumann formation:

$$C_D=\begin{cases}\dfrac{24}{Re_p}\left(1+\dfrac{Re_p^{\frac{2}{3}}}{6}\right) & when\ Re_p<1000\\ 0.424 when\ Re_p\geq 1000\end{cases} \quad (3.17)$$

The particle Reynolds number is given by:

$$Re_p = \frac{\rho_a (u_a - u_p) d_p}{\mu} \tag{3.18}$$

Where μ is molecular viscosity of the fluid in MPa-s and d_p is particle diameter in mm.

Substitute equation 3.16, 3.17 and 3.18 in to equation 3.15; the particle acceleration is given by:

$$\frac{\partial u_p}{\partial t} = \frac{3}{4}\frac{\rho_a}{\rho_p}\frac{(u_a - u_p)\left|(u_a - u_p)\right|}{d_p} + g_x \frac{(\rho_p - \rho_a)}{\rho_p} \tag{3.19}$$

The instantaneous trajectory of the particles can be calculated by integrating:

$$\frac{dX_p}{dt} = u_p \tag{3.20}$$

3.2.2 Spray breakup model

Spray atomization involves two steps: first, the liquid jet is broken up, followed by the droplets and ligaments. This research work describes the primary break-up utilising the blob method. Blobs of the same diameter as the nozzle are injected and the number of droplets injected per unit time is computed using a total mass flow rate. Injected droplets experience Kelvin-Helmholtz (KH) and Rayleigh-Taylor (RT) instability. Kelvin-Helmholtz instability exhibited due to the relative velocity between the gas and liquid phases creates shearing action on the droplet. As result the parent droplet breaks into small child droplets. This child droplets experience secondary breakup due to the combined effect of KH and RT as shown in Fig. 3.1. Rayleigh-Taylor instability is generated due to the inertia of the denser fluid. The droplet breakup process is similar in both KH and HT.

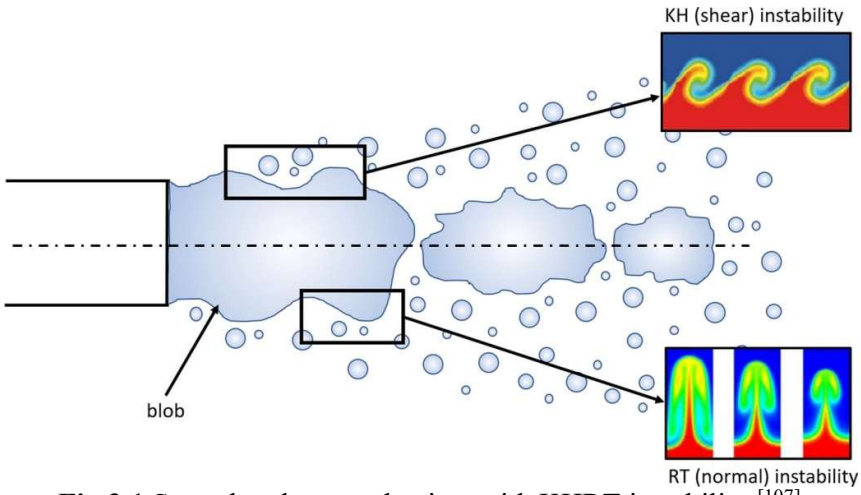

Fig 3.1 Spray breakup mechanism with KHRT instability [107]

As Weber number increases, faster aerodynamic effects led to increases the formation of the smaller droplets. The KHRT and Wave model used to calculate the aerodynamic

effects on droplet breakup. The radius of the parent droplet (r) decreases continuously during the break up until it reaches at stable radius (r_{KH}):

$$\frac{dR}{dt} = \frac{r - r_{KH}}{\tau_{KH}} \tag{3.21}$$

It is assumed that the radius of the stable droplets is directly proportional to the wavelength of the unstable surface:

$$r_{KH} = B_o \Lambda_{KH} \tag{3.22}$$

Where Λ_{KH} is the wave length, $B_o = 0.61$ model constant $\& \tau_{KH}$ is the characteristics breakup time of the droplet can be given as:

$$\tau_{KH} = \frac{3.726 B_1 r}{\Lambda_{KH} \Omega_{KH}} \tag{3.23}$$

B_1 is adjustable model constant having range in between 20 (evaporating) to 60(non-evaporating. Where Λ_{KH} is the wave length and Ω_{KH} is the frequency, which is given by Reitz et al [7]

$$\Omega_{KH} = \frac{0.34 + 0.38 We_a^{1.5}}{(1+Z)(1+1.4T^{0.6})} \sqrt{\frac{\sigma}{\rho_p r^3}} \tag{3.24}$$

$$\Lambda_{KH} = \frac{9.02 r (1 + 0.45\sqrt{Z})(1 + 0.4T^{0.7})}{(1 + 0.865 We_a^{1.67})^{0.6}} \tag{3.25}$$

Where,

$$\text{Z (Ohnesorge number)} = \frac{\sqrt{We_p}}{Re_p}$$

$$We_p (Weber\ number) = \frac{\rho_p (u_a - u_p)^2 r}{\sigma}$$

$$Re\ (Reynolds\ number) = \frac{\rho_p (u_a - u_p) r}{\mu_p}$$

$$We_a (Weber\ number) = \frac{\rho_a (u_a - u_p)^2 r}{\sigma}$$

$$T\ (Taylor\ number) = Z\sqrt{We_a}$$

The wave length and frequency for RT (Rayleigh-Taylor) model is given by:

$$\Lambda_{KH} = 2\pi \sqrt{\frac{3\sigma}{a(\rho_p - \rho_a)}} \tag{3.26}$$

$$\Omega_{KH} = \sqrt{\frac{2}{3\sqrt{3\sigma}} \frac{(a(\rho_p - \rho_a))^{1.5}}{(\rho_p - \rho_a)}} \tag{3.27}$$

Where ‘a’ is the droplet acceleration is calculated by:

$$a = \frac{3}{8} C_D \frac{\rho_a (u_a - u_p)^2}{\rho_p r} \tag{3.28}$$

However, droplets breakup rate in RT (Rayleigh-Taylor) model is too fast, hence model should apply after breakup length (L_b) from the nozzle outlet. The breakup length is:

$$L_b = C D_{nozzle} \sqrt{\frac{\rho_p}{\rho_a}} \tag{3.29}$$

Where C is the model constant (for non-evaporating=20)

3.3 TWO-STEP COUPLING METHOD

The two-step coupling method is a novel computational approach that links the internal flow parameters of a fuel injector nozzle to its external spray formation and breakup. This method is particularly effective for understanding how cavitation within the nozzle affects spray dynamics, which is critical for optimizing fuel injectors and improving engine efficiency.

Step-1: Internal flow simulation

- Multiphase CFD simulation:

In the first step, a computational fluid dynamics (CFD) simulation is performed to model the cavitation flow inside the injector nozzle. This is often achieved by a homogeneous Eulerian multi-fluid technique. In this method, the two phases are considered to be the same fluid. Often, liquid viscosity, surface tension and relative velocity are neglected, and the pressure of the mixture is assumed to be the saturation pressure. The volume of fluid (VOF) with the sharp inter-phase option is used as a multiphase model. The mass transfers between the two phases are governing by the cavitation mechanism. For cavitation modelling the Zwart-Gerber-Belamri (ZGB) cavitation model is used. This will calculate the formation and collapse of cavitation bubbles based on vapour pressure and local pressure. Simulation is performed using inlet pressure and atmospheric outlet boundary conditions. The steady flow simulation is considered to extract the data at the outlet of the nozzle.

- Extracting data

Once internal flow simulation is completed, key parameters are extracted. The parameters at the outlet of the nozzle have been calculated and an injection file has been created for spray simulation. These include coordinate position, velocity, diameter, temperature, and mass flow rates. These parameters are calculated in each grid cell of the outlet cross-section and then stored in a *.inj file. The total number of grid cells at the outlet is 150, and for each cell, a parameter has been obtained assuming a steady-state condition. In the current work, a steady

file was employed to avoid handling enormous amounts of data and reduce computational time. The steady file for a file injection requires the following format:

```
((x y z u v w diameter temperature mass-flow) name)
```

Where x, y, and z are the position coordinates and u, v, and w is the velocity in respective dimensions. All of the words represent numerical parameters in scientific floating-point notation in SI units. All parentheses are necessary, but the name is optional. The second file has been created for the turbulent kinetic energy (ε) and turbulent dissipation rate (ω) in terms of profile data at the nozzle outlet.

Step-2: External spray simulation

- Initial condition:

For spray simulation, a Lagrangian-based DPM model has been used. ANSYS-Fluent's discrete phase calculations depend on initial conditions defining particle stream positions, velocities, and physical effects, which may require additional particle properties. To specify the initial conditions for a particle/droplet stream, create an "injection" and assign properties to it. In present method injection is assigned in terms of “file injection” type. The file injections may work in two ways, depending on the file format: A steady file can be applied to both steady and unsteady particle tracking. In the former instance, each line entry in the file generates a new particle parcel for each injection time step, as normal. By default, injection time steps match global fluid-flow time steps. An unstable file is only suitable for unsteady particle tracking. Each line entry in the file includes a time step. The turbulent kinetic energy (ε) and turbulent dissipation rate (ω) is assigned at the inlet boundary condition using profile data.

- Spray breakup modelling:

The primary and secondary breakup of fuel jet is modelled using the Kelvin-Helmholtz Rayleigh-Taylor (KHRT) model. This model simulates the instability of a liquid jet that leads to disintegration into droplets. In the Lagrangian approach, individual droplets are tracked as they move through the surrounding air. This approach allows for detailed analysis of droplet behaviour. The final stage is to examine the spray characteristics, such as penetration length, spray angle, and droplet size distribution. The impact of internal cavitation on these parameters is evaluated, providing information about how cavitation enhances or hinders spray breakup.

Advantages of two-step coupling method:

(1) Computationally efficient: Separating the simulation into two steps allows for efficient use of computational resources. Complex cavitating flow can be tackled with

specialized techniques in step 1, while spray tracking in step 2 can be done with a different approach.

(2) Better Accuracy: The two-step coupling method is more accurate at predicting spray characteristics than simpler models because it explicitly considers the influence of cavitation on the exiting jet properties.

The two-step coupling method is a powerful tool for linking internal nozzle flow characteristics with external spray dynamics. By leveraging detailed CFD simulations and advanced spray breakup models, it provides a comprehensive understanding of how cavitation and other flow phenomena within the nozzle affect spray formation. The method is particularly useful for studying the behavior of alternative fuels such as biodiesel. Since biodiesel has different physical properties compared to conventional diesel, understanding its flow and spray characteristics through this method can lead to the development of fuel injectors optimized for biodiesel use. The conceptual diagram for proposed method is shown in Fig.3.2.

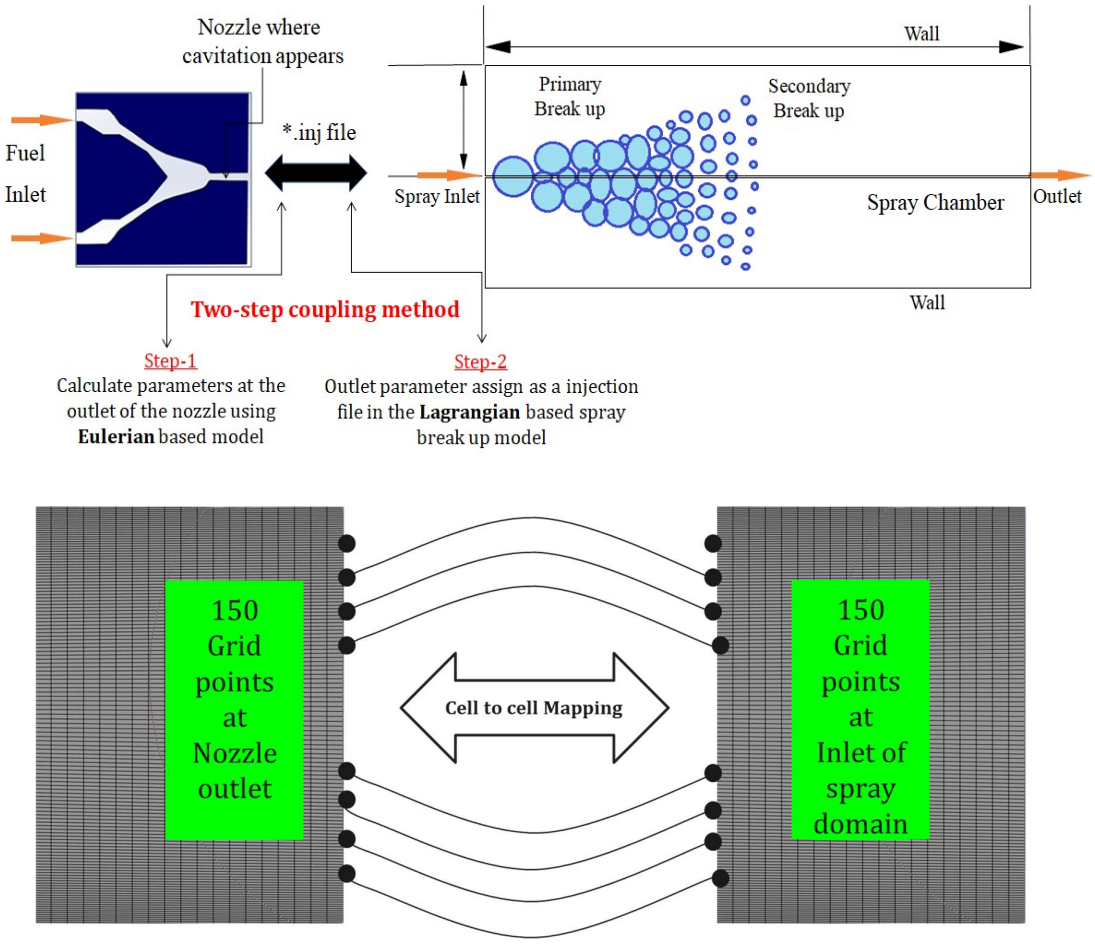

Fig.3.2 Conceptual diagram of the Two-step cavitation coupled spray breakup method

3.4 EXPERIMENTAL APPARATUS FOR CAVITATION

The schematic of the experimental setup is illustrated in Fig. 3.3. The actual experimental setup is shown in Fig. 3.4, in which filtered liquid was discharged into ambient air through custom-designed different test pieces of cavitation nozzles. The liquid flow was powered by a three-cylinder plunger pump, which could deliver pressures up to 35 bar and flow rates of 30 litres per minute (LPM) at full capacity with water. The pump was connected to a high-pressure galvanized iron pipe. This pipe included an upstream air release valve, an acrylic body rotameter for measuring flow rates up to 30 LPM (with a pressure capacity of 35 bar), and a pressure gauge with a range of 0-10 bar. The water was collected in a 50-litre reservoir tank after passing through the test pieces (nozzle outlet). This tank also supplies water back to the pump inlet. To capture high-resolution images of cavitation phenomena and liquid jets, a dedicated lighting setup and black background sheets were deployed in conjunction with a digital camera. This comprehensive imaging system facilitated the detailed analysis of cavitation and liquid jet dynamics.

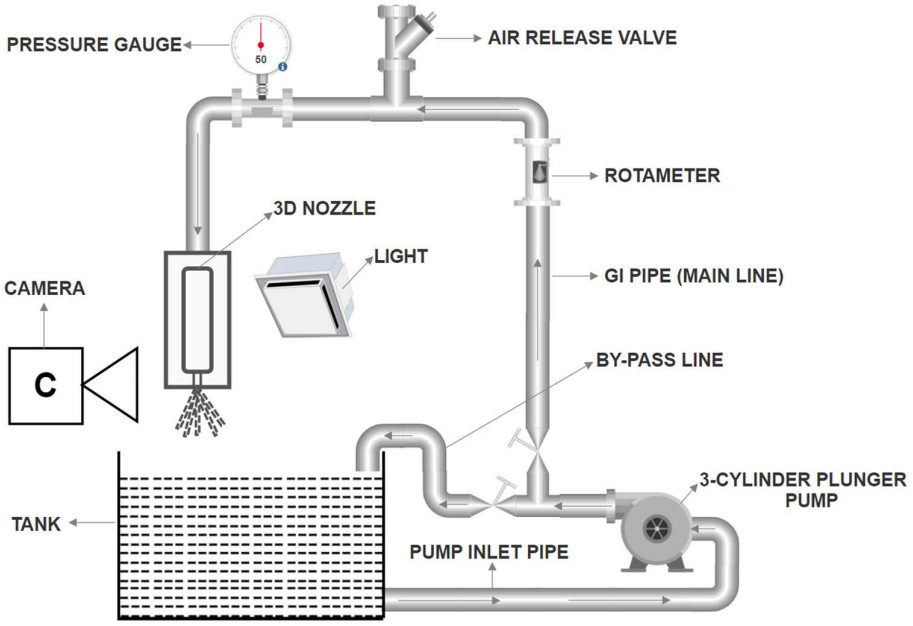

Fig. 3.3 Schematic diagram for test set up to visualization of cavitational flow

3.4.1 Development of cavitation nozzle

The design of the nozzle is crucial in facilitating optical access for visualizing cavitation flow within the experimental setup. To achieve this, careful consideration was given to various design parameters to ensure optimal performance and visualization capabilities. Furthermore, nozzle must withstand high pressure liquid flow during the operation. The inlet and outlet sections of the nozzle are precisely machining to facilitate cavitation formation and its effect

on spray formation. Different possibility of nozzle design has been explored in this research work.

The First cavitation nozzle (CN1) was made from an 8mm thick stainless-steel plate. After machining, the stainless steel was covered with a 5mm thick acrylic plate on both sides, as shown in Fig. 3.5. However, with the current experimental setup, CN1 did not create cavitation. The CFD simulation shows that the length upstream from the nozzle is insufficient to create fully developed flow. The nozzle's hydraulic diameter is not small enough to accelerate flow at its entry. To address this issue, the second cavitation nozzle (CN2) is made from a 2 mm thick stainless-steel plate. The angle of divergence is sufficient for recovering the pressure loss, as seen in Fig.3.6. However, this nozzle has an issue of leakage under high pressure flow. It has been learned that the acrylic plate fixed with industrial glue would not sustain high pressure.

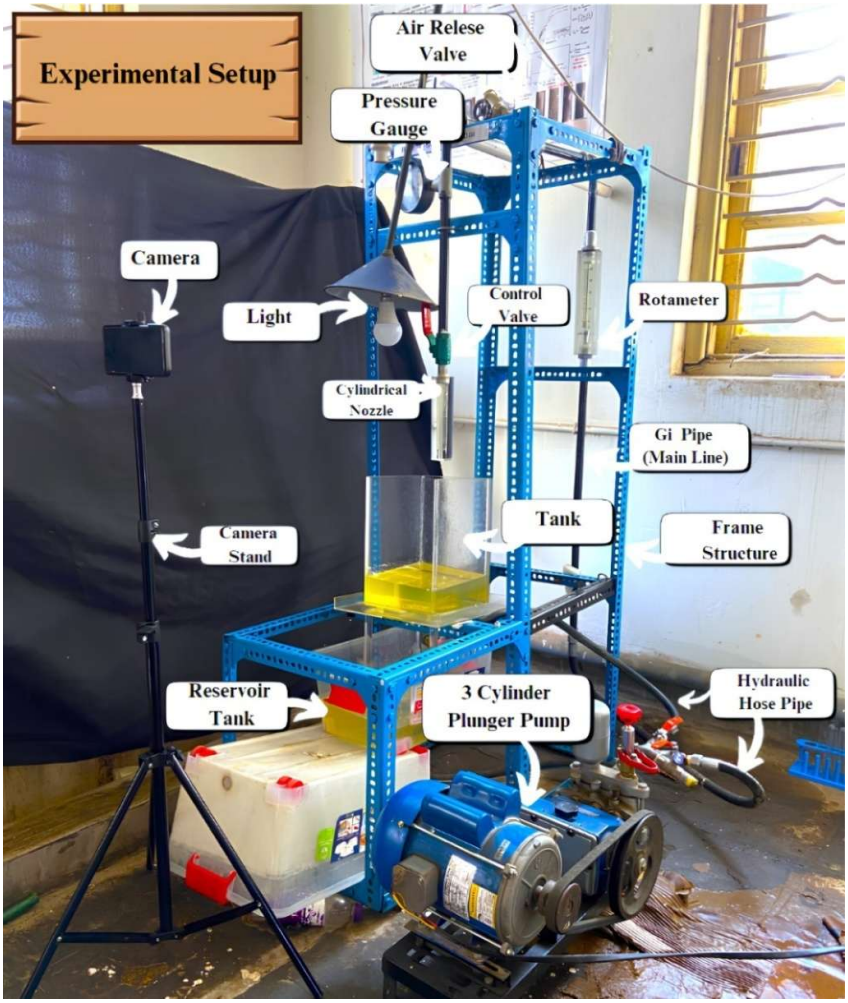

Fig. 3.4 Actual image of test set up to visualization of cavitation flow

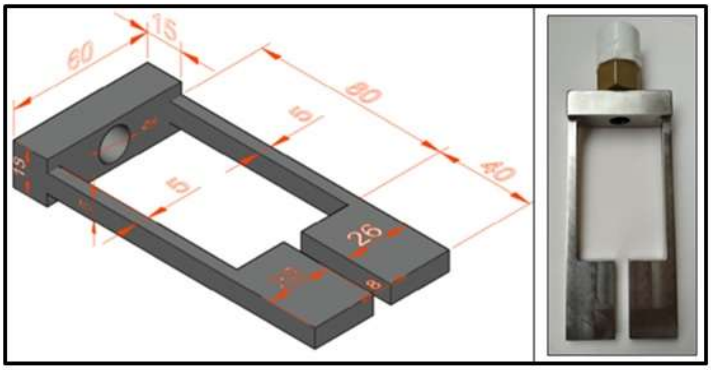

Fig. 3.5 Details of cavitation nozzle-1 (CN1), L= 10 mm, W_n=8mm, t=8mm

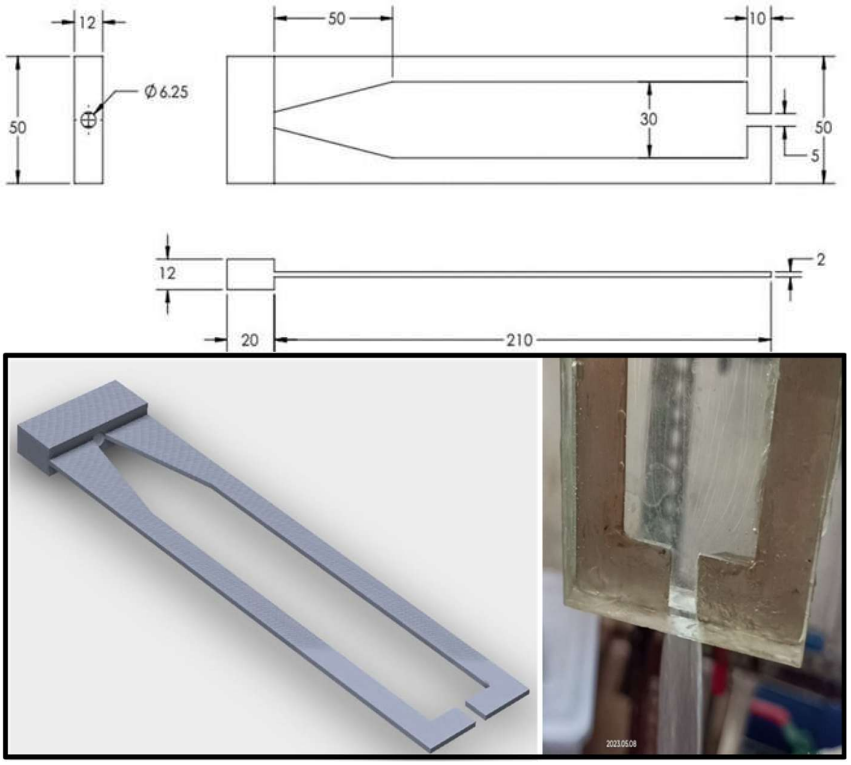

Fig. 3.6 Details of cavitation nozzle-2 (CN2), L= 10 mm, W_n =5mm, t=2mm

Finally, the third cavitation nozzle (CN3) was meticulously developed with high-precision on an aluminium block using a vertical machining centre (VMC machine), resulting in an outstanding accuracy level of 1 micrometre. The CN3 is equipped with an upstream reservoir that maintains consistent injection pressure before fluid enters the nozzle. The nozzle body was anodized in black colour to increase durability and contrast with the whitish cavitation cloud. For optimal visualization of the fluid flow through the nozzle, a 10 mm-thick acrylic plate, affixed with an Allen head bolt as shown in Fig.3.7 and 3.8. The dimensions of the nozzle were estimated using a 'Mitutoyo 3D microscope' (with a minimum

count of 0.1 micrometres) as shown in Fig. 3.9. The results show an extremely steep corner at the entrance of the nozzle.

The cavitation map was created using CN3. It is believed that the specific stage of cavitation, namely super cavitation, contributes to an increase in spray cone angle. To demonstrate this, a special purpose cavitation nozzle 4 (CN4) has been developed as shown in Fig. 3.10. This nozzle is designed so that super cavitation occurs on one side while no cavitation emerges on the other side at the same injection pressure. This nozzle confirms that the increase in spray cone angle is due to super cavitation alone, not pressure rise.

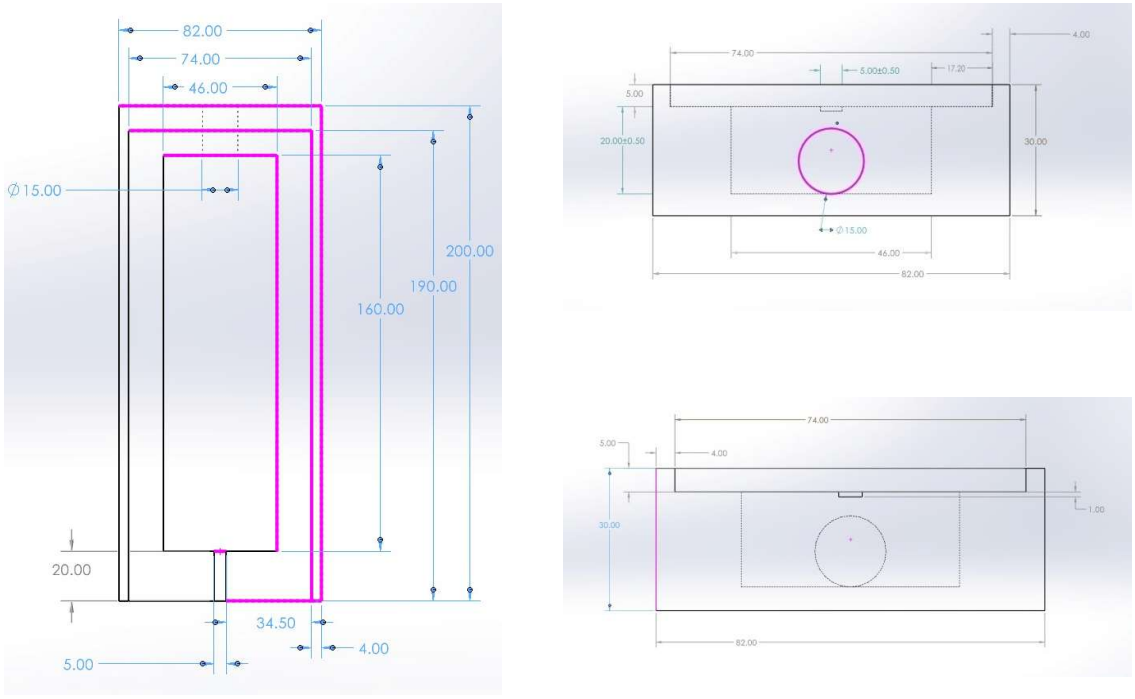

Fig. 3.7 Schamatic diagram of cavitation nozzle 3 (CN3)

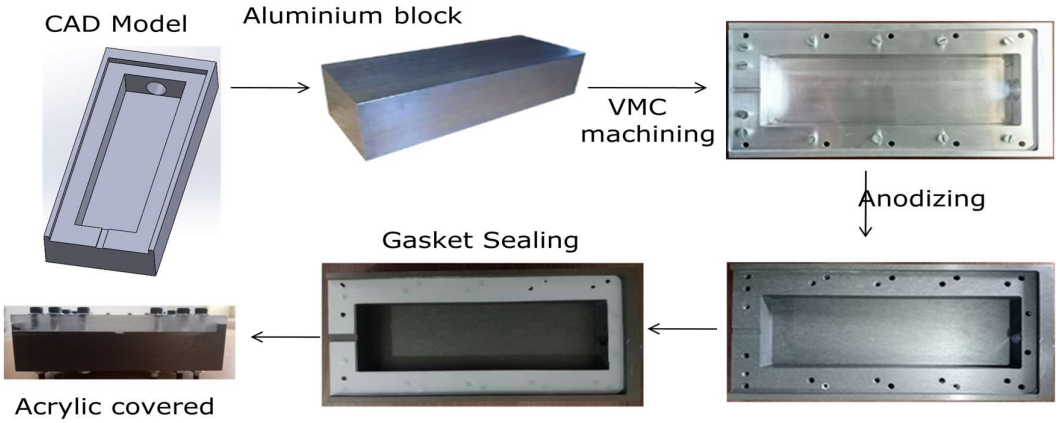

Fig.3.8 Development stages of the cavitation nozzle-3 (CN3)

Inlet

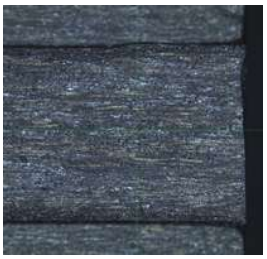

Outlet

Fig. 3.9 Microscopic image of the cavitation nozzle-3(CN3)

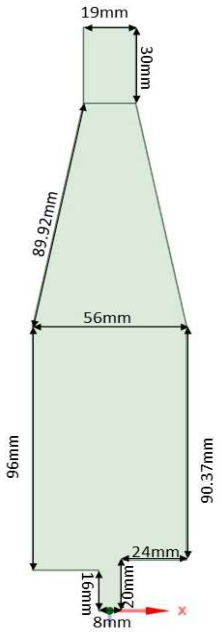

Dimension of Cavitation nozzle-4

Cavitation nozzle-4with anodizing

Left side of the nozzle

Right side of the nozzle

Microscopic image of the cavitation nozzle-4

Fig. 3.10 Details of cavitation nozzle-4(CN4)

The cylindrical-shaped cavitation nozzle-5 (CN5) is a simplified and bigger variant of the fuel injector nozzle. It was constructed from a solid acrylic bar that was precisely drilled all the way through, as illustrated in Fig. 3.11. It was carefully polished with fine cotton fabric to remove surface imperfections and increase transparency.

3.4.2 Experimental conditions

The cavitation phenomenon is dependent on the geometrical and operating parameters. The current study considers the effect of geometry in the form of the nozzle's length to diameter (L/W) ratio. The operating conditions vary with injection pressure. The atmospheric pressure is considered as 1.013 bar. The entire experimental work was conducted using three different liquids: water, diesel, and biodiesel (tallow biodiesel and WCO biodiesel). The fluid properties are listed in Table 3.2. Details of the typical experimental conditions are provided in Table 3.3

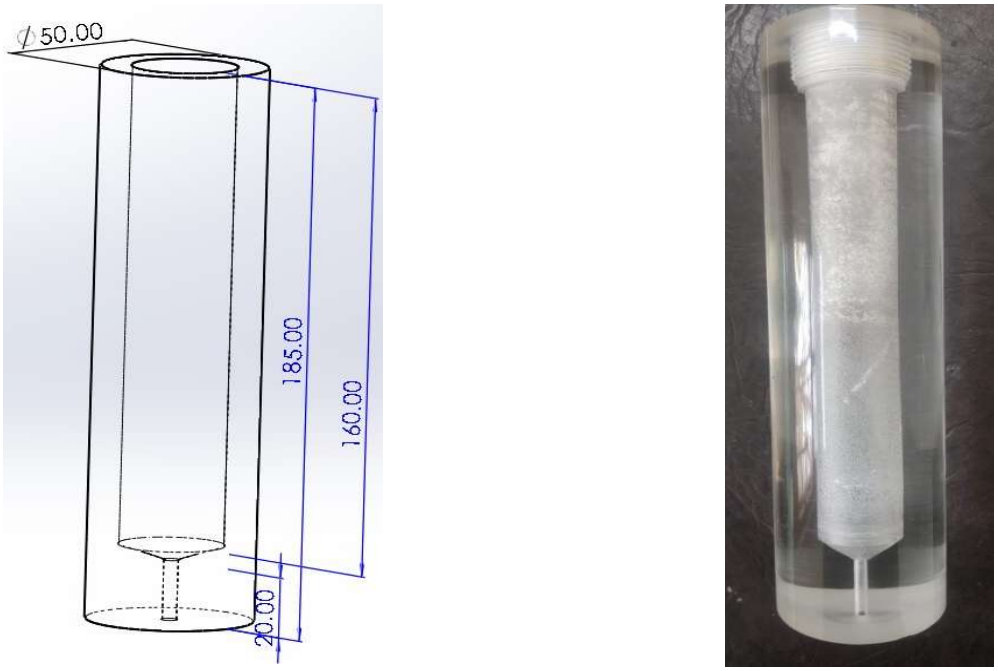

Fig. 3.11 Details of cavitation nozzle-5(CN5)

Table 3.2 Liquid properties

Fluid Properties	Water	Diesel	WCO Bio-diesel	Tallow Bio-diesel
liquid density (ρ) (kg/m^3)	1000	830	886/853	873
liquid Kinematic viscosity (cP)	1	2.3	4.03	4.6
liquid Dynamic viscosity (Pa s)	0.000798	0.001517	0.00453	-
vapor pressure (P_v) (Pa)	4000	2000	1000	1000
Surface tension (N/m)	0.072	0.025	0.0296	0.03

Table 3.3 Experimental conditions

Sr. No.	Nozzle type	Nozzle L/W Ratio	Liquid Used	Temperature (T_i-T_f) Range ($°C$)	Pressure (P_i-P_f) Range (bar)	Flow rate (Q_i-Q_f) Range (LPM)
1	CN 3W	4	Water	29 – 34	0.7 – 5.8	3 – 7.2
2	CN 3D	4	Diesel	27 – 35	0.6 – 5.5	3 – 8
3	CN 3B	4	Bio-Diesel	28 – 36	0.6 – 5	4 – 8
4	CN 4W	-	Water	29 – 34	0.4 - 9.6	3 – 16
5	CN 5W	8	Water	29 – 32	0.7 – 7.9	3 – 7.7
6	CN 5D	8	Diesel	27 – 32	0.6 – 5.6	3 – 8
7	CN 5B	8	Bio-Diesel	28 – 32	0.5 – 5.6	3 – 8

3.5 EXPERIMENTAL APPARATUS FOR SPRAY CHARATCTERISTICS

The experiment used a Delphi make single-hole injector with a 0.2mm nozzle diameter. The injector operated at a maximum working pressure of 500 bar. To regulate injection pressure, a motor-driven fuel pump was used. The spray parameters of diesel and biodiesel fuels were investigated, including penetration length and spray cone angle. The motor powered a fuel pump that transferred fuel from the fuel tank. The setup involved two injectors. Injector 1 functioned as a nozzle, while Injector 2 collected the fuel supplied, allowing for the measurement of flow -rate. The fuel pump functioned as a distribution pump, ensuring that both injectors received an equal volume and pressure. To monitor the injection pressure, a pressure gauge was installed at Injector 2. After each run, the fuel collected from Injector 2 was measured, and Injector 1's injection spray video was captured. This information made it easier to calculate the amount of fuel collected and the time it took, allowing us to determine the flow rate at particular pressures.

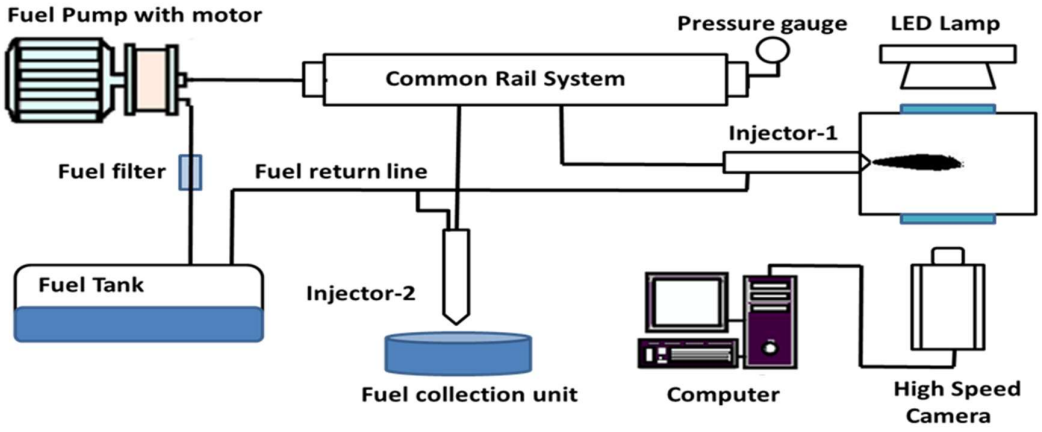

Fig 3.12 Schematic diagram of test set up to visualization of spray characteristics

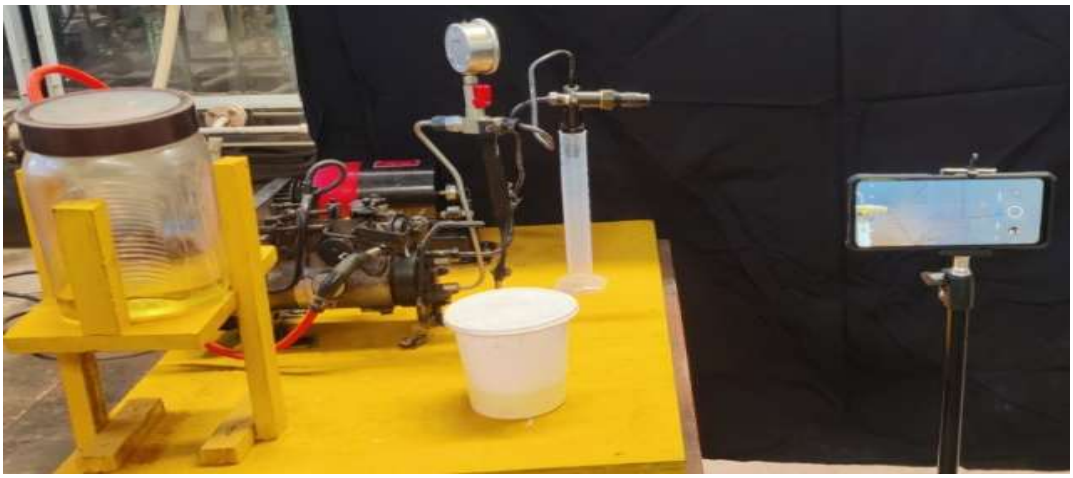

Fig. 3.13 Actual image of test set up to visualization of spray characteristics

Four fuel blends were used to evaluate cone angle and spray penetration (B00, B10, B20, and B100). The schematic diagram of the set-up is shown in Fig. 3.12 and the actual image is shown in Fig. 3.13.

3.5.1 Image processing methods

To analyse the spray characteristics in this study, a high-speed video recording camera was employed to capture the spray evolution at 1000 frames per second (fps). By integrating high-speed imaging, DaVinci Resolve for video processing, and Python-based image analysis using the Otsu method, a systematic and precise approach was developed for evaluating spray characteristics. This method provides a reliable way to study cavitation-induced spray behavior, offering valuable insights into the fuel injection process.

Step-1: DaVinci Resolve for Video Processing

DaVinci Resolve is a professional-grade video editing and post-processing software widely used for high-resolution video manipulation. In this study, it was utilized to process high-speed video recordings of spray injection, captured at 1000 frames per second (fps). The software's advanced playback and timeline control features allowed for 100x slow-motion processing, enabling the extraction of intermediate frames for further analysis. DaVinci Resolve's frame-by-frame precision ensured that each stage of spray development was accurately captured. Additionally, its color grading and noise reduction tools enhanced image clarity, improving the quality of extracted frames before applying further image processing techniques.

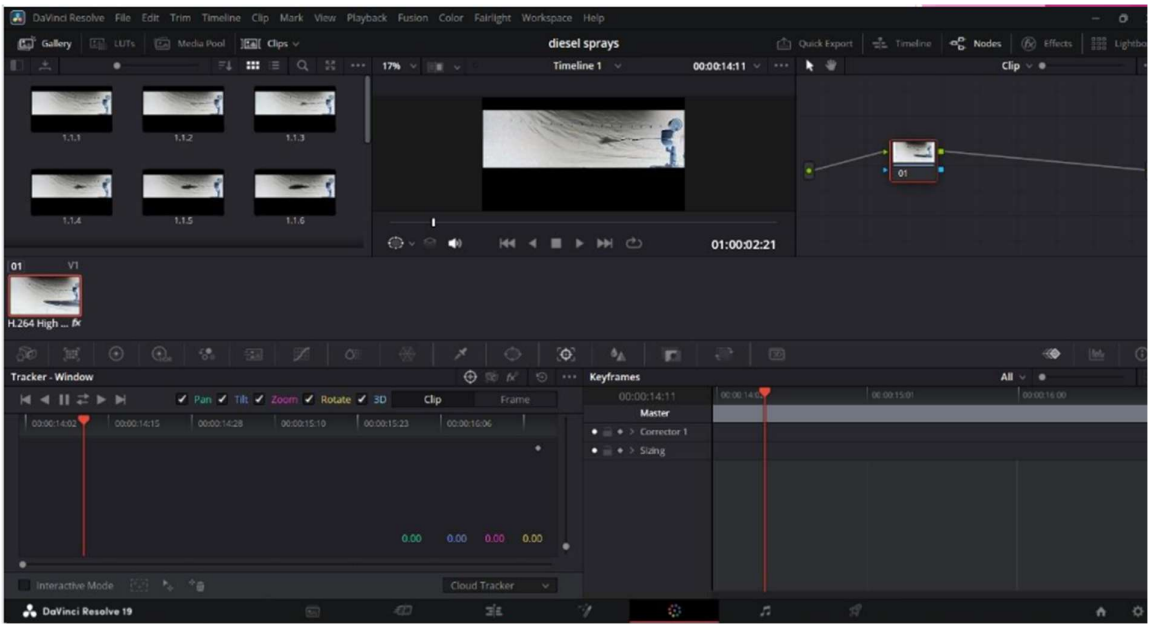

Fig. 3.14 Graphic user interface of DaVinci Resolve

Step-2: Python for Image Processing

Python was employed for automated image analysis, leveraging its powerful libraries for numerical computing and image manipulation. The extracted frames were processed using OpenCV (Open-Source Computer Vision Library), which provides robust tools for image segmentation, thresholding, and measurement. The Otsu method, a widely used automatic thresholding algorithm, was implemented to convert grayscale images into binary images. Grey scale image has only one channel and the intensity of each pixel is represented by a single value between 0 and 255. This method determines an optimal threshold by minimizing intra-class variance, ensuring precise differentiation between the spray and background. The binary image conversion allowed for clear edge detection, which is essential for analysing spray morphology.

Step-3: Measurement of Spray Characteristics

Once the binary images were obtained, Autodesk Inventor, a CAD-based software, was used to accurately measure spray cone angle and spray tip penetration. To determine the spray angle for small size nozzles, use the angle generated by tangent lines travelling through the nozzle tip and along the spray surface's border in the stable area. This region refers to the conical section of the spray immediately after exiting the nozzle, which varies in length depending on injection conditions. Baumgarten C. [4] estimated its length to be 50% of the jet penetration and used this length of spray to estimate the spray angle.

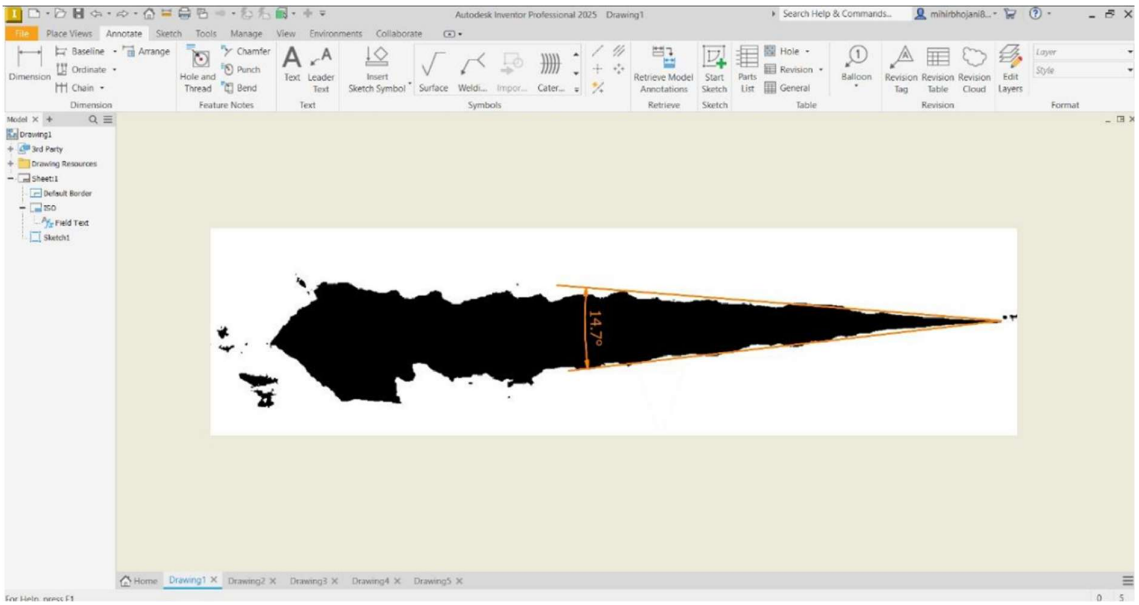

Fig 3.15 Graphic user interphase of Autodesk Inventor

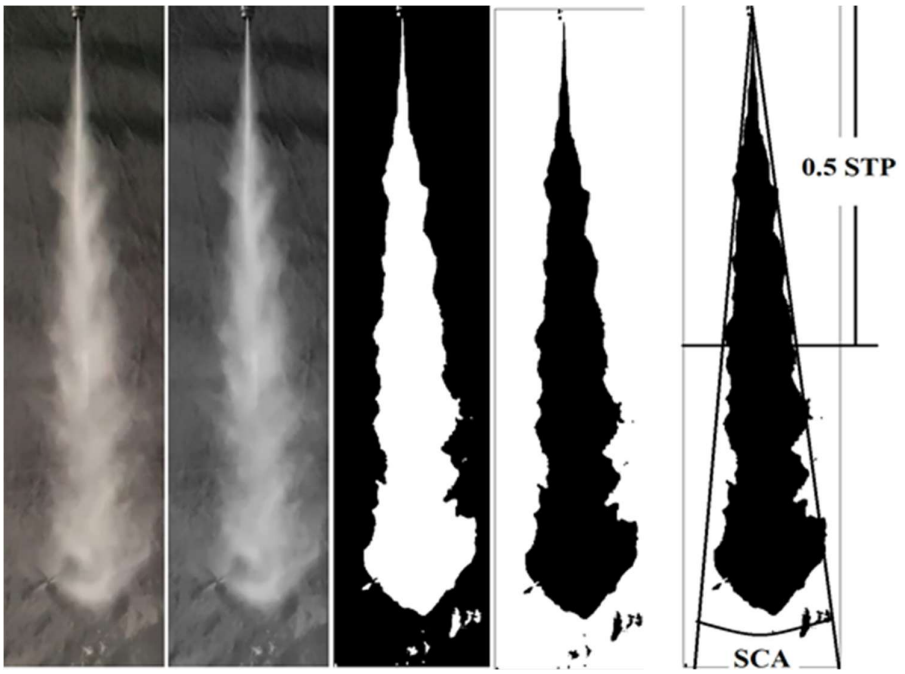

Fig. 3.16 Image processing steps

3.6 BIODIESEL PRODUCTION FROM WASTE COOKING OIL (WCO)

As explained in Chapter 1, hydrodynamic cavitation (HC) is a highly energy-efficient biodiesel production technology. An in-house technology has been developed for producing biodiesel from waste cocking oil. Hydrodynamic cavitation is achieved by employing an office-type cavitation reactor. A thorough study was conducted to optimize the cavitation reactor and the production time of WCO biodiesel. Fig. 3.15 and 3.16 depict the experimental setup for biodiesel production from WCO.

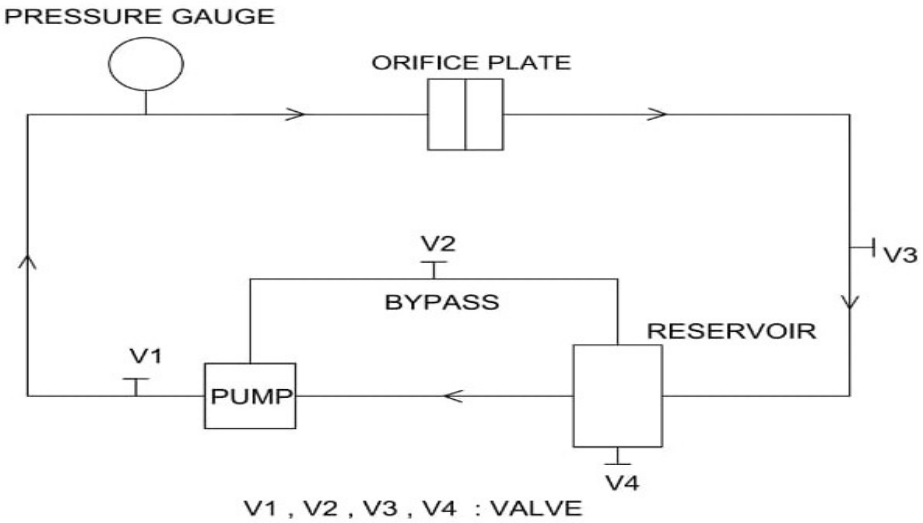

Fig 3.17 Schematic diagram of experimental setup for biodiesel production using hydrodynamic cavitation

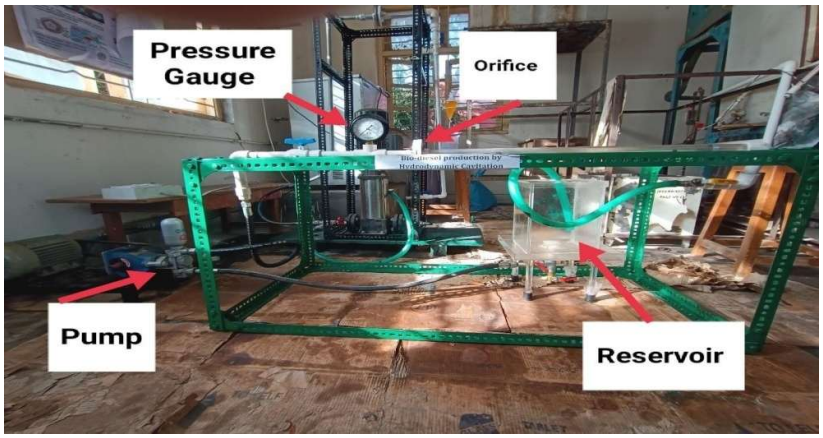

Fig 3.18 Actual image of experimental setup for biodiesel production using hydrodynamic cavitation

Initially, 5.5 litres of waste cooking oil were purchased from a local vendor in Vadodara. The initial free fatty acid (FFA) content had been determined in the chemistry lab and it was 2.7 KOH/gm, which is within the acceptable limit for biodiesel generation using the hydrodynamic cavitation method. Preheating the oil to 110˚C removes moisture. Then WCO and methanol were combined at a 6:1 molar ratio. In the present investigation, 1% NaOH was used as a catalyst. The combination is then passed through the experimental test apparatus, with samples collected every 5 minutes to determine the time required to complete the reaction.

3.7 CLOSER

This chapter provides thorough information on the computational and experimental approaches employed in current research. The present numerical approaches reviewed include multiphase models, turbulence models, cavitation models, and discrete phase models. The 'Two-Step Coupling Method' is innovative for calculating cavitation-coupled spray breakup. The project includes developing an experimental setup for cavitation flow visualization and spray development. The final portion discusses the in-house developed biodiesel producing unit. Validating numerical and experimental results against benchmark experimentation or analytical data is essential. The extensive validation is discussed in the following chapter. The newly developed two-step coupling method has been compared with the published method. In-house experiments were also conducted to validate the suggested approach.